Chapter 3

An *in situ* Surface-Enhanced Raman Spectroelectrochemical Analysis System with Hemin Modified Nanostructured Gold Surfaces*

An integrated surface-enhanced Raman scattering (SERS) spectroelectrochemical (SEC) analysis system is presented that combines a small volume microfluidic sample chamber (< 100 μL) with a compact three-electrode configuration for *in-situ* surface-enhanced Raman spectroelectrochemistry. The SEC system includes a nanostructured Au surface that serves dual roles as the electrochemical working electrode (WE) and SERS substrate, a microfabricated Pt counter electrode (CE), and an external Ag/AgCl reference electrode (RE). The nanostructured Au WE enables highly sensitive *in situ* SERS spectroscopy through large and reproducible SERS enhancements, which eliminates the need for resonant wavelength matching of the laser excitation source with the electronic absorption of the target molecule. The new SEC analysis system has the merits of wide applicability to target molecules, small sample volume, and a low detection limit. We demonstrate *in situ* SERS spectroelectrochemistry measurements of the metalloporphyrin hemin showing shifts of the iron oxidation marker band $\nu 4$ with the nanostructured Au working electrode under precise potential control.

* This chapter is based on T. Yuan, L. L. Thi Ngoc, J. Nieuwkasteele, M. Odijk, A. van den Berg. H. Permentier, R. Bischoff, E. T. Carlen. *In situ* surface-enhanced Raman spectroelectrochemical analysis system with a hemin modified nanostructured gold surface. Anal. Chem. 87 (2015) 2588-2592, and
L. L. Thi Ngoc, T. Yuan, N. Oonishi, J. Nieukasteele, A. van den Berg, H. Permentier, R. Bischoff, E. T. Carlen. Suppression of surface-enhanced Raman scattering on gold nanostructures by metal adhesion layers. J. Phys. Chem. C. 120 (2016) 18756-18762.

3.1 Introduction

Spectroelectrochemistry combines conventional electrochemistry with optical spectroscopy, which provides a more complete description of chemically driven electron transfer processes and redox events. *In situ* Raman spectroelectrochemistry is particularly important for understanding electrode processes at the interface of a WE and sample solution [1]. With the WE under potential control, electrochemistry can provide thermodynamic and kinetic information of chemical processes, while *in situ* Raman spectroscopy provides molecular vibrational information indicative of structure and conformation. The discovery of SERS on nanostructured metal surfaces, which is due to the large enhancement of the inelastic scattering cross-section of a molecule at the metal surface, has enabled the determination of structural information of adsorbed molecules at very low concentrations using Raman spectroscopy [2-4]. The combination of surface-enhanced Raman spectroscopy and electrochemistry has been shown to be a powerful tool to monitor *in situ* structural changes of surface adsorbates or reaction intermediates [5-9]. The application of spectroelectrochemistry for the investigation of redox processes is of great interest, especially when the processes can be triggered electrochemically through precise control of the WE potential.

Resonance Raman spectroscopy and *in situ* surface-enhanced Raman spectroelectrochemistry have been applied extensively to redox-active proteins, heme proteins and metalloporphyrins [10-19]. However, in most cases surface-enhanced resonance Raman scattering (SERRS), excited with high laser powers, is required in order to detect small quantities of adsorbed species on the WE [10-17]. SERRS requires that the laser source wavelength is resonant with the surface plasmon resonance wavelength of the nanostructured metal surface as well as the electronic absorption band of the molecule of interest, thus SERRS spectroelectrochemistry is most often performed on Ag nanostructures, which are prone to oxidation in aqueous solutions. The SERRS requirement limits *in situ* Raman spectroelectrochemistry to molecules with absorption wavelengths in the visible spectrum, and the high laser powers can affect thermally and photochemically sensitive redox systems in an uncontrolled manner.

In this chapter, we present an *in situ* SERS spectroelectrochemical (SEC) analysis system that is comprised of a microfluidic sample chamber integrated with a compact three-electrode configuration. The WE and CE are microfabricated on a silicon

substrate that is directly bonded to the microfluidic chamber. The WE is a SERS-active nanostructured Au surface that has been recently reported by our research group [20]. The nanostructured Au WE surfaces provide reproducible SERS enhancements on the order of 10^8 that can be precisely tuned to the incident laser wavelength. Therefore, resonance Raman excitation is no longer required to achieve a reasonable signal to noise ratio, which allows the use of a Au WE. Additionally, the small sample volume microfluidic chamber is especially suitable for the analysis of hazardous or costly samples.

3.2 Experimental Section

Reagents. 4-Mercaptopyridine (MPy), dimethyl sulfoxide (DMSO), NaH_2PO_4, Na_2HPO_4, 30% H_2O_2 and concentrated H_2SO_4 are analytical grade and purchased from Sigma-Aldrich (Munich, Germany). Hemin (H651-9, Frontier Scientific, USA) was used without further purification. Water was purified by a Maxima Ultrapure water system (ELGA, High Wycombe, Bucks, UK).

SEC chip fabrication. Figure 1 shows the SEC chips fabrication process. A 40 nm thick low stress silicon nitride (SiN) layer was first deposited onto the silicon wafer by low-pressure chemical vapor deposition (Figure 1a). Next, a positive photoresist was spin-coated on the SiN layer and patterned with conventional contact ultraviolet lithography, and subsequently developed. After the development step, a 5 nm Cr and 100 nm Pt metal stack was deposited on the wafer by sputtering, and followed by a lift-off process with acetone, ultrasonication, and rinsing with deionized water (Figure 1b). There was a 1.5 mm separation gap at the center of the chip between the Pt electrodes where the nanostructured WE was to be fabricated. The wafer was then cut into 5 pieces (chips). The chips were then cleaned in a 3:1 mixture of piranha (H_2SO_4: 30% H_2O_2). The nanopatterned SiN template surfaces were then formed over a 0.5×0.5 mm area at the center of the chip between the Pt electrodes (Figures 1c-1e) (see the details of the fabrication of the nanostructured gold surface in the following section). The final step of the SEC chip fabrication was the deposition of the nanostructured Au WE. A custom-made shadow mask (0.1 mm thick sheet of Ni) with a square hole (1 mm^2) at its center was used to selectively deposit Au on the nanopatterned SiN region to form the nanostructured Au WE. A 60 nm Au layer, (with a thin Ti adhesion layer to prevent delamination,) was deposited (sputtering with DC source in Ar plasma) on the SiN template to form the SERS-active WE. The Au layer partially overlaps one of the Pt electrodes for external electrical

connection to the potentiostat (Figure 1f and 1g). The Ti adhesion layer is very thin (deposition rate: 0.06 nm s^{-1} and deposition time: 3 s) to prevent plasmon damping. The microfluidic chamber was fabricated from a 3 mm thick layer of polydimethylsiloxane (PDMS). A 3 mm diameter hole was punched (ϕ3.0 mm Unicore, Harris) in the PDMS layer to form a cylindrical well (21 mm^3). The patterned PDMS layer was then bonded to the SEC chip by applying pressure (Figure 1h). The SEC chips can be used multiple times by replacing the Ti/Au WE layer and the PDMS microfluidic chamber.

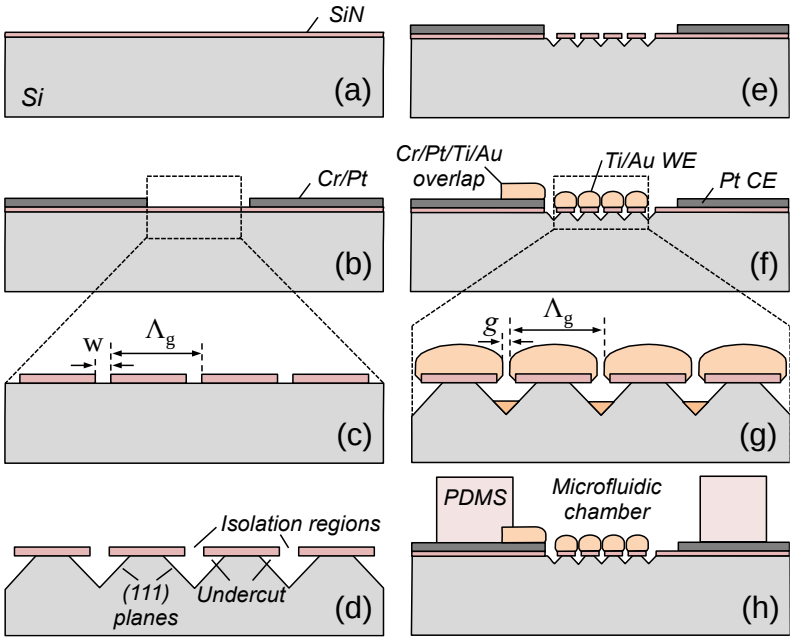

Figure1. SEC chip fabrication process steps. See text for clarification of the individual steps (a) to (h).

Nanostructured gold working electrode fabrication. A 100 nm polymethyl methacrylate (PMMA, MicroChem Corp.) electron-sensitive photoresist was spin-coated on a silicon substrate and exposed to a 130 pA electron beam with the area dose in the range of 90-120 μA s cm^{-2} (FEI Sirion UHR-SEM). The electron-beam exposure along the length of the SiN template was aligned to the [110] direction of the (100) silicon wafers using the wafer flat as a reference. The total template surface array of 1 mm^2 is written in 0.1×0.1 mm sections. The exposed regions were developed in a 1:3 methyl isobutyl ketone: isopropanol solution for 30 s, followed by immersion in isopropanol. The exposed SiN regions were removed using reactive

ion etching (60 W, 25 sccm CHF_3 and 5 sccm O_2), followed by removal of the remaining PMMA and surface cleaning with oxygen plasma. Prior to silicon etching, the native oxide on the exposed silicon regions was removed by immersion in 1% hydrofluoric acid solution for 1 min, and subsequent rinsing with deionized water. The silicon was etched in a 1% KOH solution at 55 ℃ with stirring for 45 s and rinsed with deionized water for 2 min. The different crystal planes etch anisotropically by hydroxide ions in an alkaline solution where (111) planes have the lowest etch rate and (100) and (110) planes both have higher etch rates. The surfaces were then cleaned in a 3:1 piranha solution (H_2SO_4:30% H_2O_2) for 15 min, rinsed with deionized water for 2 min, and dried with N_2. The Ti and Au film stack is deposited by sputtering (DC source) in an Ar plasma (Au deposition rate: 0.06 nm s^{-1} and Ti deposition rate: 0.06 nm s^{-1}) deposition.

SERS WE modification. Electrochemical measurements were performed on a conventional Au disk electrode, while the nanostructured Au electrode was used for the *in situ* SEC measurements. The conventional Au disk electrode (1.6 mm diameter) was polished (Micromesh microcloth, Grade 3200) with alumina slurry (0.05 μm diameter particles), and followed by sonication in water, ethanol, and water, each for 1 min. The Au electrode was then immersed in a 3:1 piranha solution (H_2SO_4:30% H_2O_2), and washed thoroughly with deionized water and dried with N_2. Following the cleaning step, the Au electrode was immersed in a 1 mM MPy in ethanol solution for 4 h, followed by 1 min sonication in ethanol, to form the self-assembled monolayer (SAM) on the Au surface. (Figure 2). After drying the MPy modified Au electrode with N_2, it is immersed in a hemin solution (1 mM in DMSO) for 18 h. Before use, the hemin modified electrode (MPy/hemin) was sonicated for 1 min in DMSO and water, respectively. The nanostructured Au WE was prepared and modified with the MPy/hemin layer using a similar protocol.

Working electrode preparation and modification. Two working electrodes were used for the experiments. Electrochemical measurements were performed on the Au disk electrode while the nanostructured Au surface was used for the *in situ* SEC measurements. A conventional Au disk electrode (Bioanalytical Systems, Inc.) with 1.6 mm diameter was polished with a microcloth (Micromesh Grade 3200) and alumina slurry (0.05 μm diameter particles), and subsequently sonicated in water, ethanol and water, each for 1 min. The Au electrode was then immersed in a 3:1 piranha solution (H_2SO_4:30% H_2O_2), and washed thoroughly with deionized water and dried with N_2. The workflow of the electrode modification is displayed in Figure

2. First, the Au electrode was immersed in 1 mM 4-mercaptopyridine (MPy) in ethanol for 4 h, followed by 1 min sonication in ethanol. After drying the MPy modified Au electrode with N_2, it was immersed in a hemin solution (1 mM in DMSO) for 18 h. Before use, the hemin modified electrode was sonicated in DMSO and water, each for 1 min. The nanostructured Au WE was modified with the MPy/hemin layer using a similar protocol.

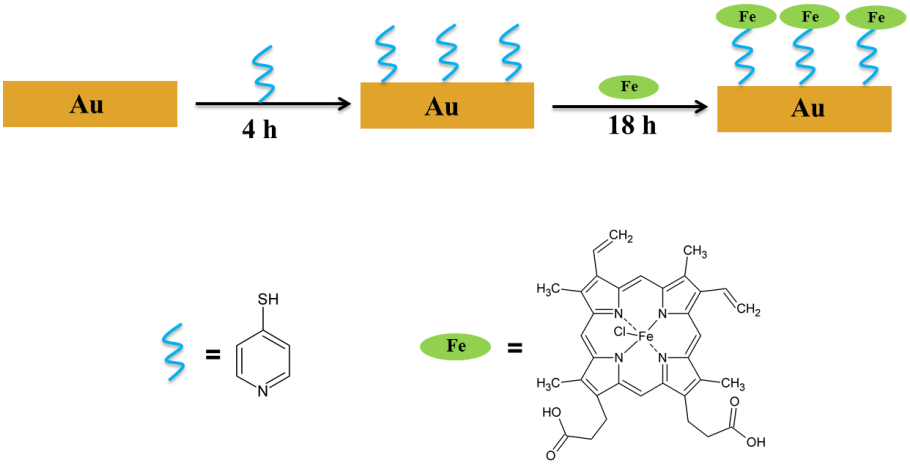

Figure 2. Workflow of the preparation of the 4-Mercaptopyridine (MPy)/hemin modified gold electrode.

Raman scattering measurement instrumentation. A confocal Raman microscope system (alpha300R, Witech GmbH) was used for the Raman scattering measurements, which is comprised of a TE-cooled charge coupled device (DU970P-BV, Andor Technology, Belfast, Northern Ireland), UHTS300 spectrometer (f/4 300 mm FL; grating: 600 lines mm^{-1}), fiber-coupled confocal configuration with 50 μm core diameter, and fiber coupled laser excitation through a $\lambda/2$ rotator plate for polarization control and laser focusing with the microscope objective. The spectral resolution of the spectrometer is ±3 cm^{-1}. Elastically scattered light is removed with an edge filter. A He-Ne (1.96 eV/632.8 nm) laser source in a backscatter configuration was focused on the surfaces using a 40×/0.8 NA dipping microscope objective (Nikon, Fluor).

SERS measurements. The surface plasmon resonance energy was tuned to the laser excitation energy (to maximize the SERS enhancement) by controlling the pitch and nanogap width (Figure 1) through controlling the nanostructured Au layer thickness, which was verified with reflectance measurements. The SERS spectra of the MPy

and MPy/hemin modified nanostructured Au surfaces were measured in aqueous sodium phosphate buffer with a laser power of 0.2 mW (the laser power was measured at the entrance of the microscope objective). The integration time for the MPy modified electrode measurements was 3 s and the integration time for the MPy/hemin modified electrode measurements was 10 s. Spatial imaging was performed over a 5×5 μm area.

Electrochemical instruments and measurements. Electrochemical measurements were performed with a potentiostat (VSP 200, Bio-Logic SAS, France). A batch cell system with conventional three-electrode configuration consisting of the conventional Au WE (1.6 mm diameter, MF-2014, Bioanalytical Systems, Inc.) and Pt wire (MW-4130, Bioanalytical Systems, Inc.) CE was used for control experiments. All potentials were measured against an Ag/AgCl RE (MF-2079, BaSi). A 25 mM sodium phosphate buffer (pH 7.0) was used as the supporting electrolyte. The SEC-chip was clamped and bonded to a custom-made printed circuit board and spring-loaded Cu clips provided the electrical connection from the microfabricated Pt electrodes to the Cu trace on the circuit board. Conventional coaxial cables and connectors were used to connect the SEC-cell to the potentiostat.

3.3 Results and Discussion

3.3.1 *In situ* SERS SEC system

The *in situ* SERS SEC system consists of a SEC-cell optically interfaced to the Raman microscope, and electrically interfaced to a potentiostat, as shown in Figure 3a. The SEC-cell is comprised of an on-chip nanostructured Au WE and microfabricated Pt CE, directly bonded to the microfluidic sample chamber that is optically interfaced to the Raman spectrometer via a dipping microscope objective (Figure 3b). An external Ag/AgCl wire RE is inserted directly into the microfluidic chamber (Figure 3c). A representative scanning electron microscopy (SEM) image of a nanostructured Au WE surface is shown in Figure 3d. The peak surface plasmon resonance wavelength of the nanostructured Au WE is tuned to coincide with the He-Ne laser excitation wavelength of 632.8 nm to ensure an optimal SERS enhancement [19]. Additionally, a thin Ti adhesion layer is deposited prior to the Au deposition to prevent delamination during WE modification. The nanostructured Au WE is first modified with the 4-Mercaptopyridine self-assembled monolayer (MPy SAM). Hemin is subsequently added to the MPy surface, which was previously

reported to form a coordinative bond between the iron core of the heme and the nitrogen of the MPy SAM [14, 21-22].

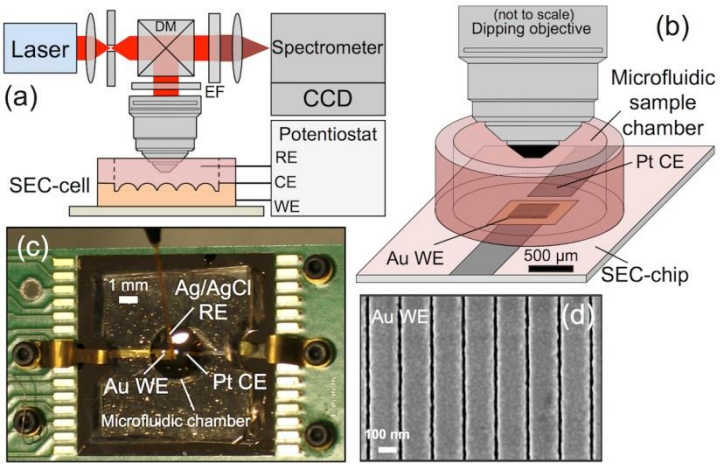

Figure 3. *In situ* SERS SEC analysis system. (a) Schematic representation of the Raman SEC analysis system, (b) SEC-cell comprised of a SEC-chip directly bonded to a small-volume microfluidic sample chamber with an optical interface to a microscope objective, (c) SEC-cell consisting of a Pt CE and a nanostructured Au WE patterned on the silicon SEC-chip, and an external Ag/AgCl RE, (d) Representative SEM image of the nanostructured Au WE.

3.3.2 Electrochemical characterization of the hemin modified gold electrode

The electrochemical characteristics of the hemin modified electrode were first investigated on a conventional Au disk electrode, and subsequently reproduced on the nanostructured Au working electrode. Cyclic voltammetry (CV) was performed with 5 mM $Fe(CN)_4^{3-/4-}$ in the supporting electrolyte. The CV from an unmodified Au disk WE shows a pair of redox peaks corresponding to the Fe^{3+}/Fe^{2+} redox transitions (blue trace, Figure 4a). After incubation with MPy and hemin, the current decreased significantly (black and red traces, Figure 4a), thus demonstrating that hemin is immobilized on the MPy modified WE. In Figure 4b the CV of a MPy/hemin modified Au disk WE in argon-saturated sodium phosphate buffer with pH 7.0 (red trace) shows a well-defined, quasi-reversible redox couple (vs Ag/AgCl) from the MPy/hemin modified surface. CV of the nanostructured Au WE is shown in Figure 4c, where the anodic and cathodic peak currents increase linearly for scan rates in the range of 3-10 V s^{-1}, thus indicating that the redox reaction of the

immobilized hemin is a surface-controlled process [23], which further supports immobilization of hemin on the nanostructured Au WE. The hemin surface coverage on the nanostructured gold electrode is estimated to be 8.6×10^{-12} mol cm^{-2} [24].

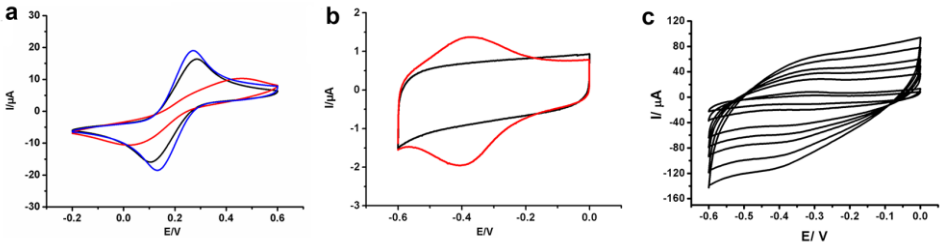

Figure 4. Cyclic voltammograms from conventional and nanostructured Au WEs. (a) Unmodified (blue), MPy modified (black), and MPy/hemin modified (red) conventional Au WE measured in 5 mM $Fe(CN)_4^{3-/4-}$ (scan rate 100 mV/s), (b) MPy modified (black) and MPy/hemin modified (red) conventional Au WE in 25 mM sodium phosphate buffer, pH 7.0 (argon saturated, scan rate 1 V/s), (c) MPy/hemin modified nanostructured Au WE in 25 mM sodium phosphate buffer (pH 7.0, argon saturated), with scan rates in the range of 3-10 V s^{-1} (inner to outer traces).

3.3.3 SERS spectra of an MPy/hemin modified nanostructured Au electrode

The SERS spectra measured from the MPy/hemin modified nanostructured Au WE using the *in situ* SERS SEC analysis system are shown in Figure 5. Figure 5a shows a schematic of the MPy/hemin modified Au WE. The SERS vibration bands of the MPy modified nanostructured Au WE are shown in the spectrum of Figure 5b, corresponding to 6a(a_1), ν(C-S)+ β(C-C) (700 cm^{-1}); 10b(b_1), γ(C-H) (778 cm^{-1}); 1(a_1), β(C-C-C) (1000 cm^{-1}); 18a(a_1), β(C-H) (1036 cm^{-1}); 12(a_1), β(C-C-C)+ν(C-S) (1094 cm^{-1}); 9a(a_1), β(C-H) (1210 cm^{-1}); 3(b_2), β(C-H) (1274 cm^{-1}); 19a(a_1), ν(C=C/C=N) (1492 cm^{-1}); 8b(b_2), ν(C-C) (1577 cm^{-1}); and 8a(a_1), ν(C-C) (1608 cm^{-1}), in agreement with previous assignments [25]. The labels γ, β, and ν indicate out-of-plane bending, in-plane bending, and stretching modes, respectively. The spatially averaged enhancement factor is in the range of 10^7-10^8, which is in agreement with previously reported values for nanostructured Au and Ag surfaces [20, 26]. The signal-to-noise ratio (SNR) is defined as $SNR = \overline{S}/\sigma$, where $\overline{S}$ is the average band intensity and σ is the amplitude of the noise signal in the region of the band [27]. For the 1(a_1) vibration mode, $SNR_{1(a1)}\approx12$, and for the 12(a_1) vibration mode $SNR_{12(a1)}\approx22$.

The SERS spectra measured from the MPy/hemin modified nanostructured Au WE are shown in Figures 5c, 5d and an enhancement is depicted in Figure 6. Since the primary scope of this work is the development of the SEC analysis system, we provide a preliminary analysis of the measured SERS spectra of the MPy/hemin modified WE. Figures 5c and 5d depict SERS spectra for WE potentials E=-0.2 V and E=-0.5 V (vs. Ag/AgCl), respectively. Many of the MPy vibration bands are observed in the SERS spectra, such as 700 cm^{-1} 6a(a_1), 1000 cm^{-1} 1(a_1), and 1094 cm^{-1} 12(a_1). Certain vibrational modes of the porphyrin ring of hemin have been observed to shift in frequency consistent with the oxidation state, axial ligation, or coordination, and spin state of the central iron atom [11-15, 28-29]. The ν(C-C) and ν(C-N) stretch vibrations of the porphyrin ring are typically observed to shift in frequency according to the iron oxidation state, which occur in the marker band range of 1300-1700 cm^{-1}. The ν_4 (A_{1g}) vibration mode is due mainly to C-N stretch vibrations of the pyrrole subunits that are sensitive to electron transfer in the π^* orbital of the porphyrin ring [30], and is an indicator of the iron oxidation state. The ν_4 mode is observed in the frequency range of 1368-1377 cm^{-1} for ferric (Fe^{3+}) hemin and in the range of 1344-1364 cm^{-1} for ferrous (Fe^{2+}) hemin [18, 31].

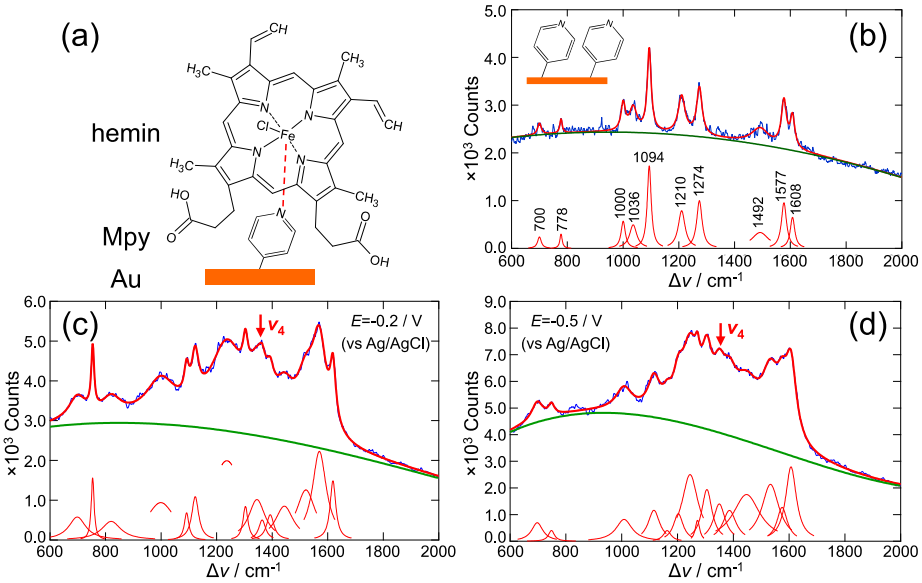

Figure 5. SERS spectra of a nanostructured Au WE under potential control in 25 mM sodium phosphate buffer. (a) Schematic of the MPy/hemin modified Au surface, (b) SERS spectrum of MPy modified Au surface, (c) SERS spectrum of MPy/hemin modified Au surface with *E*=-0.2 V, (d) SERS spectrum of MPy/hemin modified Au surface with *E*=-0.5 V. Blue traces: raw data, red traces: modeled data, and green traces: modeled background (the vibration bands are modeled with a Lorentzian band shape after subtraction of the background using a cubic polynomial function).

In Table 1, assignments of the measured spectra from MPy modified nanostructured Au surfaces are listed [32]. Preliminary assignments of the measured spectra from MPY/hemin modified nanostructured Au surfaces are listed in Table 2.

Table 1. Raman band assignments from MPy modified nanostructured Au surfaces. The labels γ, *β,* and ν indicate out-of-plane bending, in-plane bending, and stretching modes, respectively. Laser power: 0.2 mW and 3 s integration time.

Band (cm^{-1})	**Assignment**[3]
700	$6a(a_1)$, ν(C-S)+ β(C-C)
778	$10b(b_1)$, γ(C-H)
1000	$1(a_1)$, β(C-C-C)
1036	$18a(a_1)$, β(C-H)
1094	$12(a_1)$, β(C-C-C)+ν(C-S)
1210	$9a(a_1)$, β(C-H)
1274	$3(b_2)$, β(C-H)
1492	$19a(a_1)$, ν(C=C/C=N)
1577	$8b(b_2)$, ν(C-C)
1608	$8a(a_1)$, ν(C-C)

Table 2. Raman band assignments from MPy/hemin modified nanostructured Au surfaces. Laser power: 0.2 mW and 10 s integration time. NA indicates not assigned. Hemin mode assignments ν_2, ν_3, ν_4, ν_{10}, ν_{15}, ν_{20}, ν_{21}, and ν_{22} from Sanchez and Spiro [33], and Hu *et al*. [34].

***E*=-0.2 V**			***E*=-0.5 V**		
Band (cm^{-1})	**Band area**	**Assignment**	**Band** (cm^{-1})	**Band area**	**Assignment**
698	67797	MPy, 6a(a_1)	697	53731	MPy, 6a(a_1)
753	31141	hemin, ν_{22} (B_{1g})[8]	748	16538	hemin, ν_{22} (B_{1g})[8]
820	62381	NA	-	-	-
999	190534	MPy, 1(a_1)	1008	90055	MPy, 1(a_1)
1091	21430	MPy, 12(a_1)	-	-	-
1123	51794	hemin, ν_{22} (A_{2g})[7]	1115	92383	hemin, ν_{22} (A_{2g})[7]
-	-	-	1163	21323	NA
-	-	-	1203	68978	NA
1236	471392	NA	1245	283345	NA
-	-	-	1271	24064	MPy, 3(b_2)
1303	28550	hemin, ν_{21} (A_{2g})[7]	1305	140876	hemin, ν_{21} (A_{2g})[7]
1345	102876	hemin, ν_4 (A_{1g}), Fe^{2+}	1349	114378	hemin, ν_4 (A_{1g}), Fe^{2+}
1366	23812	hemin, ν_4 (A_{1g}), Fe^{3+}	-	-	-
1393	32577	hemin, ν_{20} (A_{2g})[8]; hemin+Py[6]	1386	113532	hemin, ν_{20} (A_{2g})[8]; hemin+Py[6]
1445	112956	hemin, ν_3 (A_{1g}) + MPy 19b(b_2)[3]	1447	331564	hemin, ν_3 (A_{1g}) + MPy 19b(b_2)[3]
1521	163211	NA	1533	251298	NA
1570	213342	hemin, ν_2 (A_{1g})[7]	1574	90939	hemin, ν_2 (A_{1g})[7]
1619	58160	hemin, ν_{10} (B_{1g})[7]	1607	215321	hemin, ν_{10} (B_{1g})[7]

3.3.4 *In situ* SERS spectra in the iron marker band range

Figure 6 shows the corresponding SERS spectra in the iron marker band range. For an applied potential of *E*=-0.2 V (Figure 6a), two bands can be resolved at 1345 cm^{-1} and 1366 cm^{-1}. The $\nu_{4\text{-}1}$=1345 cm^{-1} band lies in the ferrous state range with 81% of the integrated counts, and the $\nu_{4\text{-}2}$=1366 cm^{-1} band lies in the ferric state range with 19% of the integrated counts, which indicates that most of the iron is in the Fe^{3+} stage [18], For an applied potential of *E*=-0.5 V (Figure 6b), a single vibration band is observed at $\nu_4 \approx 1349$ cm^{-1}, which lies in the reduced ferrous state range, thus indicating reduction to the Fe^{2+} state (see Table 2 for a tabulated list of the observed Raman bands).

The vibration modes ν_2 (A_{1g}), ν_3 (A_{1g}), and ν_{10} (B_{1g}), which are mainly due to the ν(C-C) stretch vibrations, are typical indicators of the coordination and spin state of the $Fe^{2+/3+}$ ions in hemin. The bands at 1570 cm^{-1} (Figure 6a, *E*=-0.2 V) and 1574 cm^{-1} (Figure. 6b, *E*=-0.5 V) are most likely associated with the ν_2 mode of hemin, which corresponds well to previous assignments of five-coordinated ferric heme with high spin state (5cHS).[32] The bands at 1619 cm^{-1} (Figure. 6a, *E*=-0.2 V) and 1607 cm^{-1} (Figure 6b, *E*=-0.5 V) are likely associated with the ν_{10} (B_{1g}) mode of ferrous hemin, which also correspond well to previous assignments of 5cHS heme [32]. It is important to note that the ν_2 and ν_{10} modes overlap the MPy ring stretch ν(C-C) modes 8b(b_2) at 1577 cm^{-1} and 8a(a_1) at 1608 cm^{-1} (Figure 6b), respectively. The broad vibration modes at 1445 cm^{-1} (Figure 6a, *E*=-0.2 V) and 1447 cm^{-1} (Figure 6a, *E*=-0.2 V) may be due to a combination of the in-plane ring stretching mode of MPy 19b(b_2) near 1450 cm^{-1} [25], and the ν_3 (A1g) mode near 1495 cm^{-1} of hemin, but this requires further investigation before definitive assignments can be made [35]. The bands at 1392 cm^{-1} and 1387 cm^{-1} are not currently assigned, but were previously observed in SERRS spectra of hemin adsorbed on Ag surfaces in the presence of pyridine [36]. It is important to note that these observations and assignments are preliminary.

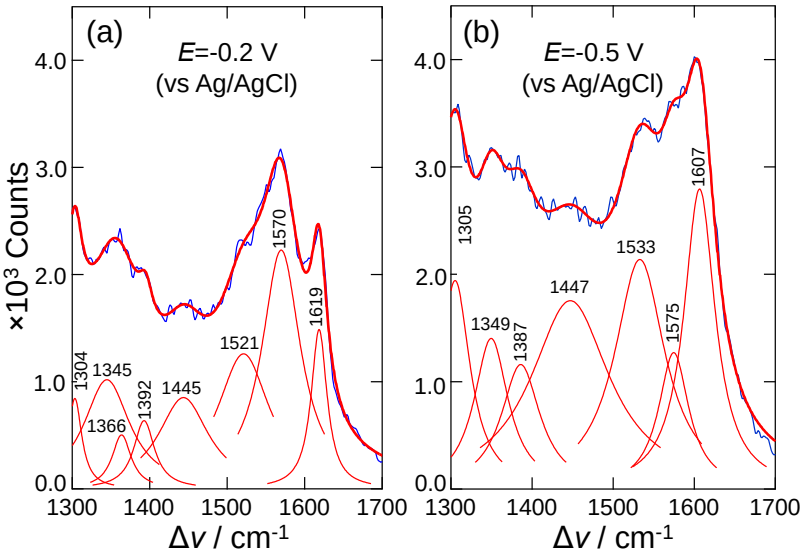

Figure 6. SERS spectra from MPy/hemin modified nanostructured Au WE in the marker band region (background corrected). (a) Electrode potential *E* = -0.2 V, (b) Electrode potential *E* = -0.5 V. Raw data: blue traces and modeled data: red traces.

3.3.5 Enhancement factor estimations

The mean and variance of the spatially averaged SERS enhancement factor are estimated from measurements of benzenethiol self-assembled monolayers on Au and Ag nanostructured surfaces and liquid neat benzenethiol. Since SERS is used for surface-enhanced Raman spectroscopy, the analytical enhancement factor for a specific vibrational mode at each measurement location (x_i, y_i) is estimated with $Y_i \approx (\kappa_i/N_{SERS})(\kappa_{CR}/N_{CR})^{-1}$, where κ_i and κ_{CR} are the integrated intensities from the SERS and conventional Raman measurements, respectively. N_{SERS} and N_{CR} are the number of molecules in the collection volume of each measurement, respectively. It should be noted that N_{SERS} is estimated from a monolayer on the SERS substrate surface. 200 SERS spectra from a Raman image were modeled using Lorentzian peak shapes and a cubic polynomial function for background subtraction. The κ_i of each band is estimated for each of the *i* measurements using modeled bands. The number of molecules within the collection volumes for each measurement of benzenethiol is $N_{SERS}=D_sA_s$, where D_s [unit: molecules/cm^{-2}] is the surface density of the molecules and A_s is the collection area of the microscope objective. The collection area can be estimated as $A_s \approx \pi R_d^2$, where R_d is the radius of the diffraction limited spot size of the microscope objective, which can be estimated from $2R_d=D_d \approx 1.27\lambda/\text{N.A.}$, where λ is the wavelength of the laser source, in this case λ=632.8 nm, and N.A. is the numerical aperture of the microscope objective, in this case N.A.=0.8. Therefore, $A_s \approx 1\times10^{-12}$ m^2, assuming that the spot size diameter is 1 μm.

3.3.6 Suppression of SERS on gold nanostructures by metal adhesion layers

The damping of surface plasmon resonance (SPR) in Au thin films by Ti and Cr adhesion layers was addressed by the biosensing community over twenty years ago [37]. It is now common practice to manufacture SPR biosensors with ultrathin (1-2 nm) Ti adhesion layers with approximately 50-nm thick Au layers, which offers a reasonable trade-off between plasmon damping and adhesion strength of the metal layer to glass substrates [38]. Plasmon damping by metal adhesion layers has been recently rediscovered in PC-Au nanostructures [39]. However, in the experiment, we found that the SERS signals varied according to the thickness of the Ti layer. Ti adhesion layers broaden and redshift the localized surface plasmon resonance (LSPR) band, as well as suppress SERS on PC-Au nanostructures. For Au

nanostructures with dimensions more than 50 nm, ultrathin Ti layers (~1-2 nm) do not significantly dampen the LSPR and SERS and provide a good trade-off between SERS enhancement and substrate reliability.

3.4 Conclusions

In conclusion, we present a new *in situ* SERS spectroelectrochemical analysis platform that is comprised of a small volume sample chamber and a nanostructured Au working electrode, which allows for the simultaneous SERS and electrochemical investigation of any modified electrode surface with very low laser power. Ultrathin Ti offers high SERS enhancement, as well as stability. The nanostructured Au working electrode has a large and reproducible SERS enhancement, which enables highly sensitive surface-enhanced Raman spectroscopy without resonant excitation of the molecule of interest, thus simplifying the measurement apparatus and expanding the applicability to a wider range of target molecules.

References

[1] W. Plieth, G. S. Wilson, C. G. De La Fe, Spectroelectrochemistry: A survey of *in situ* spectroscopic techniques (Technical report), SpectroPure & Appl. Chem. 70 (1998) 1395-1414.

[2] M. Fleischmann, P. J. Hendra, A. J. McQuillan, Raman-spectra of pyridine adsorbed at a silver electrode. Chem. Phys. Lett. 26 (1974) 163-166.

[3] M. Moskovits, Surface-enhanced spectroscopy. Rev. Mod. Phys. 57 (1985) 783-826.

[4] S. M. Nie, S. R. Emery, Probing single molecules and single nanoparticles by surface-enhanced Raman scattering, Science. 275 (1997) 1102-1106.

[5] I. C. G. Thanos, An in-situ Raman spectroscopic study of the reduction of HNO_3 on a rotating silver electrode, J. Electroanal. Chem. 200 (1986) 231-247.

[6] T. Itoh, T. Maeda, A. Kasuya, *In situ* surface-enhanced Raman scattering spectroelectrochemistry of oxygen species, Faraday Discuss. 132 (2006) 95-109.

[7] D. Y. Wu, J. F. Li, B. Ren, Z. Q. Tian, Electrochemical surface-enhanced Raman spectroscopy of nanostructures, Chem. Soc. Rev. 37 (2008) 1025-1041.

[8] K. S. Joya, H. J. M. de Groot, Electrochemical *in situ* surface enhanced Raman spectroscopic characterization of a trinuclear ruthenium complex, Ru-red, J. Raman. Spectroscopy. 44 (2013) 1195-1199.

[9] S. Hy, Felix, Y. H. Chen, J. Y. Liu, J. Rick, B. J. Hwang, *In situ* surface enhanced Raman spectroscopic studies of solid electrolyte interphase formation in lithium ion battery electrodes, J. Power Sources. 256 (2014) 324-328.

[10] T. M. Cotton, S. G. Schultz, R. P. Van Duyne, Surface-enhanced resonance Raman scattering from cytochrome c and myoglobin adsorbed on a silver electrode, J. Am. Chem. Soc. 102 (1980) 7960-7962.

[11] L. A. Sanchez, T. G. Spiro, Surface-enhanced Raman spectroscopy as a monitor of iron (Ⅲ) protoporphyrin reduction at a silver electrode in aqueous and acetonitrile solutions-vibronic resonance enhancement amplified by surface enhancement. J. Phys. Chem. 89 (1985) 763-768.

[12] P. Hildebrandt, M. Stockburger, Cytochrome-c at charged interfaces.1. Conformational and redox equilibria at the electrode electrolyte interface probed by surface-enhanced resonance Raman-spectroscopy. Biochemistry. 28 (1989) 6710-6721.

[13] S. Lecomte, H. Wackerbarth, T. Soulimane, G. Buse, P. Hildebrandt, Time-resolved surface-enhanced resonance Raman spectroscopy for studying electron-transfer dynamics of heme proteins, J. Am. Chem. Soc. 120 (1998) 7381-7382.

[14] D. H. Murgida, P. Hildebrandt, J. Wei, Y. F. He, H. Y. Liu, D. H. Waldeck, Surface-enhanced resonance Raman spectroscopic and electrochemical study of cytochrome c bound on electrodes through coordination with pyridinyl-terminated self-assembled monolayers. J. Phys. Chem. B. 108 (2004) 2261-2269.

[15] D. Millo, A. Bonifacio, A. Ranieri, M. Borsari, C. Gooijer, G. van der Zwan, Voltammetric and surface-enhanced resonance raman spectroscopic characterization of cytochrome c adsorbed on a 4-mercaptopyridine monolayer on silver electrodes, Langmuir 23 (2007) 4340-4345.

[16] M. Grosserueschkamp, C. Nowak, W. Knoll, R. L. C. Naumann, Time-resolved surface-enhanced resonance Raman spectro-electrochemistry of heme proteins, Int. J. Spectrosc. 24 (2010) 125-129.

[17] K. Sengupta, S. Chatterjee, S. Samanta, A. Dey, Direct observation of intermediates formed during steady-state electrocatalytic O_2 reduction by iron porphyrins. Proc. Natl. Acad. Sci. U.S.A. 110 (2013) 8431-8436.

[18] Y. M. Wang, P. C. Sevinc, Y. F. He, H. P. Lu, Probing ground-state single-electron self-exchange across a molecule-metal interface, J. Am. Chem. Soc. 133 (2011) 6989-6996.

[19] W. B. Cai, I. C. Stefan, D. A. Scherson, Determination of adsorption isotherm of species adsorbed on roughened silver electrodes from *in situ* quantitative surface enhanced Raman spectroscopy, J. Electroanal. Chem. 524 (2002) 36-42.

[20] L. Le Thi Ngoc, M. L. Jin, J. Wiedemair, A. van den Berg, E. T. Carlen, Large area metal nanowire arrays with tunable sub-20 nm nanogaps, ACS Nano. 7 (2013) 5223-5234.

[21] J. J. Wei, H. Y. Liu, A. R. Dick, H. Yamamoto, Y. F. He, D. H. Waldeck, Direct wiring of cytochrome c's heme unit to an electrode: electrochemical studies, J. Am. Chem. Soc. 124 (2002) 9591-9599.

[22] D. H. Murgida, P. Hildebrandt, Electron-transfer processes of cytochrome c at interfaces. New insights by surface-enhanced resonance Raman spectroscopy, Acc. Chem. Res. 37 (2004) 854-861.

[23] A. J. Bard, L. R. Faulkner, Electrochemical Methods. 2nd Ed., John Wiley & Sons, 2001, New York.

[24] A. K. Udit, M. G. Hill, V. G. Bittner, F. H. Arnold, H. B. Gray, Reduction of dioxygen catalyzed by pyrene-wired heme domain cytochrome P450 BM3 electrodes, J. Am. Chem. Soc. 126 (2004) 10218-10219.

[25] G. Varsanyi, Vibrational Spectra of Benzene Derivatives. Elsevier, 1969, Amsterdam.

[26] J. Wiedemair, L. Le Thi Ngoc, A. van den Berg, E. T. Carlen, Surface-enhanced Raman spectroscopy of self-assembled monolayer conformation and spatial uniformity on silver surfaces, J. Phys. Chem. C 118 (2014) 11857−11868

[27] R. L. McCreery, Raman Spectroscopy for Chemical Analysis; John Wiley, Inc.: New York, 2000.

[28] T. G. Spiro, T. C. Strekas, Resonance Raman spectra of heme proteins. Effects of oxidation and spin state, J. Am. Chem. Soc. 96 (1974) 338-345.

[29] S. Choi, T. G. Spiro, K. C. Langry, K. M. Smith, Viny influences on protoheme resonance Raman spectra: Nickel (II) protoporphyrin IX with deuterated vinyl groups, J. Am. Chem. Soc. 104 (1982) 4337-4344.

[30] T. Kitagawa, Y. Mizutani, Resonance Raman spectra of highly oxidized metalloporphyrins and heme proteins, Coord. Chem. Rev. 135 (1994) 685-735.

[31] M. L. Feng, H. Tachikawa, Surface-enhanced Resonance Raman Spectroscopic characterization of the protein native stucture, J. Am. Chem. Soc. 130 (2008) 7443-7448.

[32] G. Varsanyi, Vibrational Spectra of Benzene Derivatives. Elsevier, Amsterdam, 1969.

[33] L. A. Sanchez, T. G. Spiro, Surface-Enhanced Raman spectroscopy as a monitor of iron protoporphyrin reduction at a silver electrode in aqueous and acetonitrile solutions: vibronic resonance enhancement amplified by surface enhancement. J. Phys. Chem. 89 (1985) 763-768.

[34] S. Hu, I. K. Morris, J. P. Singh, K. M. Smith, T. G. Spiro, Complete assignment of cytochrome c resonance Raman spectra via enzymatic reconstitution with isotopically labeled hemes. J. Am. Chem. Soc. 115 (1993) 12446-12458.

[35] S. Oellerich, H. Wackerbarth, P. Hildebrandt, Spetroscopic characterization of nonnative conformational states of cytochrome c, J. Phys. Chem. B, 106 (2002) 6566−6580.

[36] J. J. McMahon, S. Baer, C. A. Melendres, Surface Raman scattering and electrochemistry of iron protoporphyrin at a polycrystalline silver electrode, J. Phys. Chem. 90 (1986) 1572-1577.

[37] L. Häussling, H. Ringdorf, F. J. Schmitt, W. B. Knoll, Biotin-Functionalized Self-Assembled Monolayers on Gold: Surface Plasmon Optical Studies of Specific Recognition Reactions. Langmuir. 7 (1991) 1837-1840.

[38] H. Neff, W. Zong, A. M. N. Lima, M. Borre, G. Holzhuter, Optical Properties and Instrumental Performance of Thin Gold Films near the Surface Plasmon Resonance. Thin Solid Films. 496 (2006) 688–697.

[39] H. Aouani, J. Wenger, D. Gerard, H. Rigneault, E. Devaux, T. W. Ebbesen, F. Mahdavi, T. J. Xu, S. Blair, Crucial Role of the Adhesion Layer on the Plasmonic Fluorescence Enhancement. ACS Nano. 3 (2009) 2043-2048.